PLASMA TRANSPORT SIMULATION MODELLING FOR HELICAL CONFINEMENT SYSTEMS

K. YAMAZAKI, T. AMANO
National Institute for Fusion Science,
Nagoya, Japan

ABSTRACT. New empirical and theoretical transport models for helical confinement systems are developed on the basis of the neoclassical transport theory, including the effect of the radial electric field and of multi-helicity magnetic components as well as the drift wave turbulence transport for electrostatic and electromagnetic modes or the anomalous semi-empirical transport. These electron thermal diffusivities are compared with experimental data from the Compact Helical System which indicate that the central transport coefficient of a plasma with electron cyclotron heating agrees with the neoclassical axisymmetric value and the transport outside the half-radius is anomalous. On the other hand, the transport of plasmas with neutral beam injection heating is anomalous in the whole plasma region. This anomaly is not explained by the electrostatic drift wave turbulence models in these discharges with flat density profiles. For a detailed prediction of the plasma parameters in the Large Helical Device (LHD), 3-D equilibrium/1-D transport simulations including empirical or drift wave turbulence models are performed which suggest that the global confinement time of the LHD is determined mainly by the electron anomalous transport in the plasma edge region rather than by the helical ripple transport in the core region. Even if the ripple loss can be eliminated, the increase in global confinement is 10%. However, the rise in the central ion temperature is more than 20%. If the anomalous loss can be reduced to half of the value used in the present scaling, as is the case in the H-mode of tokamak discharges, the neoclassical ripple loss through the ion channel becomes important even in the plasma core. The 5% radial inward shift of the plasma column with respect to the major radius improves the plasma confinement and increases the fusion product by more than 50% by reducing the neoclassical asymmetric ion transport loss and increasing the plasma radius (10%).

1. INTRODUCTION

Helical confinement configurations [1] have distinct advantages in realizing steady state operation without current drive and plasma current disruptions. To demonstrate these advantages, the Large Helical Device (LHD) with a superconducting magnetic coil system [2–4] is under construction. The present confinement properties in these systems may be within the so-called L-mode range of tokamak transport, and improvement of confinement is one of the urgent issues for helical confinement systems as well as for tokamaks. Moreover, contrary to tokamak systems, helical systems are supposed to suffer from serious helical ripple diffusion in the high temperature plasma regime. The empirical scaling law (the so-called LHD scaling) [5] of the global confinement time has been obtained on the basis of several stellarator/heliotron experiments, and the gyro-reduced Bohm (GRB) scaling is discussed in Ref. [6] regarding the modification of the LHD scaling in the high density regime. Past and present medium size experiments [7, 8] suggest that the transport outside the minor half-radius is anomalous and the transport near the centre is neoclassical for plasmas with electron cyclotron heating (ECH). In plasmas with neutral beam injection (NBI), however, the whole region is anomalous. It has been attempted to obtain the spatial dependence of the empirical thermal diffusivity [9, 10].

In large next-generation helical machines with high temperature plasmas, the neoclassical ripple transport may be important even in the core region. We have developed a new simulation model for the equilibrium transport in helical confinement systems, including the effect of the change in the plasma equilibrium and the magnetic structure on neoclassical transport. However, without knowing the radial dependences of anomalous transport coefficients, it is impossible to predict whether the effect of this ripple transport compared with anomalous transport is predominant. A new model for empirical 'local' thermal conductivities is proposed for future experiments in the LHD (major radius $R \sim 4$ m, magnetic field $B \sim 4$ T, plasma minor radius $a_p \sim 0.6$ m).

In Section 2, neoclassical models of transport coefficient are described. In Section 3, anomalous transport models based on drift wave turbulence and on empirical thermal diffusivities are presented. In Section 4, the

validity of these anomalous thermal diffusivities is checked using experimental data from CHS. Section 5 presents a 1-D transport simulation modelling coupled with a 3-D plasma equilibrium and its simulation results for LHD plasmas. Section 6 gives a summary of the conclusions.

2. NEOCLASSICAL MODELS OF THERMAL CONDUCTIVITIES

The neoclassical transport losses in helical plasma configurations are divided into an axisymmetric (SYM) tokamak-like part [11, 12] and an asymmetric (ASY) helical ripple part [13, 14]. The effects of the radial electric field E_ρ ($= -e\partial\Phi/\partial\rho$) are included in the ripple transport simulation [15]. Multiple helicity effects of the magnetic field configuration [16] are taken into account in the $1/\nu$ regime by introducing the form factor ratio of the multi-helicity case to the single-helicity case, F_m/F_s. The multi-helicity form factor F_m is calculated by using the GIOTA code [17]. The asymmetric particle and heat fluxes, Γ_{ASYa} and Q_{ASYa}, of species a (electrons (a = e) or ions (a = i)) as a function of the flux averaged radial variable ρ are given [12] by

$$\Gamma_{ASYa} = -\epsilon_t^2 \epsilon_h^{1/2} v_{da}^2 n_a \int_0^\infty dx\, x^{5/2}\, e^{-x}\, \frac{\tilde{\nu}_a(x) A_a(x)}{\omega_a^2(x)} \tag{1}$$

$$Q_{ASYa} + \tfrac{5}{2}\Gamma_{ASYa} T_a = -\epsilon_t^2 \epsilon_h^{1/2} v_{da}^2 n_a T_a^2 \times \int_0^\infty dx\, x^{7/2}\, e^{-x}\, \frac{\tilde{\nu}_a(x) A_a(x)}{\omega_a^2(x)} \tag{2}$$

where

$$A_a(x) = \frac{1}{n_a}\frac{\partial n_a}{\partial\rho} - \frac{Z_a}{T_a} E_\rho + \left(x - \tfrac{3}{2}\right)\frac{1}{T_a}\frac{\partial T_a}{\partial\rho} \tag{3}$$

$$\tilde{\nu}_a(x) = \nu_a^0 x^{-1.5} \epsilon_h^{-1} \left\{ \left[\left(1 - \frac{1}{2x}\right) \mathrm{erf}(x^{1/2}) + \frac{1}{(\pi x)^{1/2}} e^{-x} \right] + \bar{Z}_a \right\} \tag{4}$$

$$x = \frac{m_a v_{tha}^2}{2T_a} \tag{5}$$

$$\omega_a^2(x) = 2.21 \frac{\tilde{\nu}_a^2}{F_m/F_s} + 1.5\,(\epsilon_t/\epsilon_h)^{1/2}(\omega_E + \omega_{Ba})^2 + (\epsilon_t/\epsilon_h)^{3/2}\left[\frac{\omega_{Ba}}{4} + 0.6\,|\omega_{Ba}|\,\tilde{\nu}_a(x)(\epsilon_h/\epsilon_t)^{3/2} \right] \tag{6}$$

$$\nu_a^0 = \frac{4\pi e^4 n_a \ln\Lambda}{m_a^2 v_{tha}^3} \tag{7}$$

Here, ϵ_t is the toroidal inverse aspect ratio (ρ/R), ϵ_h is the helical ripple modulation, n_a is the plasma density, T_a is the plasma temperature, v_{da} is the toroidal drift velocity, v_{tha} is the thermal velocity, ω_E is the E × B drift and ω_{Ba} is the ∇B drift frequency. The collision frequency $\tilde{\nu}_a$ is $\tilde{\nu}_e = \nu_{ee} + \nu_{ei}$ with $\bar{Z}_e = Z_{eff}$ for electrons and $\tilde{\nu}_i = \nu_{ii}$ with $\bar{Z}_i = 0$ for ions. In the above equations, the ν regime transport was modified according to Ref. [14]. The radial electric profile is determined by the balance between the asymmetric electron and ion loss fluxes,

$$\Gamma_{ASYe}(E_\rho) = \Gamma_{ASYi}(E_\rho) \tag{8}$$

The validity of this multi-helicity neoclassical transport has been examined by using the DKES code [18].

3. ANOMALOUS MODELS OF THERMAL CONDUCTIVITIES

3.1. Drift wave turbulence (DWT) models

3.1.1. Electrostatic DWT models

The DWT models have been successfully used to simulate tokamak discharges [19, 20]. The electrostatic models related to $\delta E \times B/B^2$ turbulent diffusion with long wavelength ($k_\perp \rho_s \sim 1/3$, $k_\perp$ being the perpendicular wavelength and ρ_s the ion Larmor radius with the ion sound velocity $(T_e/M_i)^{1/2}$) include electron or ion modes, collisionless or dissipative modes, and cylindrical, toroidal or helical modes. The diffusion coefficients of the circulating electron (CE) mode for the collisionless regime (CCE, $\nu_{ei} < \omega_{tet}$) and the collisional regime (XCE, $\omega_{tet} < \nu_{ei}$) are

$$D_{CE} = \max(D_{CCE}, D_{XCE}) \tag{9}$$

$$D_{CCE} = \frac{\omega_{*e}}{k_\perp^2}\frac{\omega_{*e}}{\omega_{tet}} \tag{10}$$

$$D_{XCE} = \frac{\omega_{*e}}{k_\perp^2}\frac{\omega_{*e}}{\omega_{tet}}\frac{\nu_{ei}}{\omega_{tet}} \tag{11}$$

where $\omega_{*e} = k_\perp T_e/L_n eB$ ($L_n = n/n'$ is the characteristic density length) and $\omega_{tet} = v_{the}(t/R)$ are the electron diamagnetic frequency and the electron toroidal transit frequency, respectively.

The diffusion coefficients of the toroidally trapped electron (TEt) mode for the collisionless regime

(CTEt, $\nu_{efft} < \omega_{*e}$) and the dissipative regime (DTEt, $\omega_{*e} < \nu_{efft} < \omega_{tet}$) are

$$D_{TEt} = \min(D_{CTEt}, D_{DTEt}) \tag{12}$$

$$D_{CTEt} = \epsilon_t^{1/2} \frac{\omega_{*e}}{k_\perp^2} \tag{13}$$

$$D_{DTEt} = \epsilon_t^{1/2} \frac{\omega_{*e}}{k_\perp^2} \frac{\omega_{*e}}{\nu_{efft}} \tag{14}$$

where $\nu_{efft} = \nu_{ei}/\epsilon_t$ is the effective toroidal collision frequency. The GRB scaling [21] coincides with this CTE mode when the ϵ_t dependence is omitted:

$$D_{GRB} = \frac{\omega_{*e}}{k_\perp^2} = D_{CTEt}\epsilon_t^{-1/2} \tag{15}$$

For these cylindrical and toroidal electrostatic DWT models we have considered the helical ripple contributions of the collisionless mode (CTEh, $\nu_{effh} < \omega_{*e}$) and the dissipative mode (DTEh, $\omega_{*e} < \nu_{effh} < \omega_{teh}$):

$$D_{TEh} = \min(D_{CTEh}, D_{DTEh}) \tag{16}$$

$$D_{CTEh} = \epsilon_h^{1/2} \frac{\omega_{*e}}{k_\perp^2} \tag{17}$$

$$D_{DTEh} = \epsilon_h^{1/2} \frac{\omega_{*e}}{k_\perp^2} \frac{\omega_{*e}}{\nu_{effh}} \tag{18}$$

where the effective helical collision frequency ν_{effh} and the electron helical transit frequency ω_{teh} are given by

$$\nu_{effh} = \nu_{ei}/\epsilon_h$$

$$\omega_{teh} = v_{the} \frac{M}{R}$$

with the helical mode number M and the electron thermal velocity $v_{the} = (2T_e/m_e)^{1/2}$.

For the ion modes, the ion temperature gradient (ITG) turbulence is important especially for flat density profiles:

$$D_{ITG} = \frac{\omega_{*e}}{k_\perp^2} \left(2 \frac{T_i}{T_e} \eta_i \frac{L_n}{R}\right)^{1/2} f_{ITGth} \tag{19}$$

$$f_{ITGth} = (1 + \exp(-6(\eta_i - \eta_{th})))^{-1} \tag{20}$$

$$\eta_i = \frac{L_n}{L_{Ti}} = \frac{n/n'}{T_i/T_i'} \tag{21}$$

We adopt the following coefficients for total anomalous transport due to electrostatic DWT modes:

$$D_{ANe} = c_{CE}D_{CE} + c_{TEt}D_{TEt} + c_{TEh}D_{TEh} \tag{22}$$

$$\chi_{ANe} = \tfrac{5}{2} D_{ANe} \left(1 + 3c_{ei} \frac{L_n}{R} \eta_i f_{ITGth}\right) \tag{23}$$

$$\chi_{ANi} = \tfrac{5}{2} (c_{ie}D_{ANe} + c_{ITG}D_{ITG}) \tag{24}$$

The coefficients c_{CE}, c_{TEt}, c_{TEh}, c_{ei}, c_{ie} and c_{ITG} are usually set to zero or unity in this paper.

3.1.2. *Electromagnetic DWT models*

Contrary to the long wavelength turbulence, the electromagnetic drift wave has a short wavelength of a collisionless skin depth c/ω_{pe} and gives rise to $v_\parallel \delta B/B$ diffusion. The diffusion coefficient is given for tokamak systems (EMt) [22] and is extended to the helical (EMh) modes as follows:

$$D_{ANe} = c_{EMt}D_{EMt} + c_{EMh}D_{EMh} \tag{25}$$

$$D_{EMt} = \epsilon_t^{1/2} \left(\frac{c}{\omega_{pe}}\right)^2 \omega_{bet} \tag{26}$$

$$D_{EMh} = \epsilon_h^{1/2} \left(\frac{c}{\omega_{pe}}\right)^2 \omega_{beh} \tag{27}$$

$$\chi_{ANe} = \tfrac{5}{2} D_{ANe} \tag{28}$$

$$\chi_{ANi} = \tfrac{5}{2} c_{ie} D_{ANe} \tag{29}$$

where the electron bounce frequencies are

$$\omega_{bet} = \epsilon_t^{1/2} v_{the} \frac{t}{R}$$

$$\omega_{beh} = \epsilon_h^{1/2} v_{the} \frac{M}{R}$$

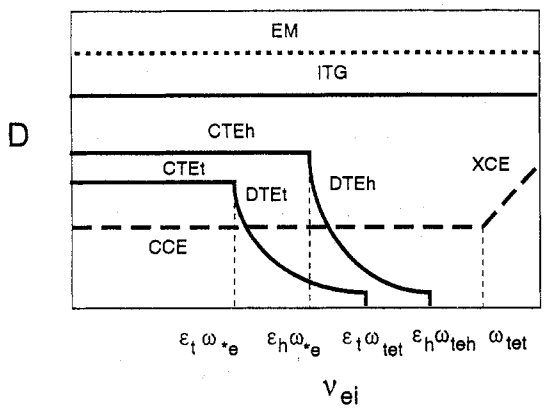

FIG. 1. Schematic drawing of transport coefficients for the DWT model. The collisionless or collisional circulating electron mode (CCE or XCE), the collisionless or dissipative trapped electron mode due to toroidicity (CTEt or DTEt), the collisionless or dissipative trapped electron mode due to helicity (CTEh or DTEh), the ion temperature gradient mode (ITG) and the electromagnetic mode (EM) are shown as a function of the collision frequency ν_{ei}.

This electromagnetic mode in tokamaks is similar to the Ohkawa model [23]

$$D_{Ohkawa} = \left(\frac{c}{\omega_{pe}}\right)^2 \omega_{tet} = D_{EMt}\epsilon_t^{-1} \quad (30)$$

which has successfully explained the ALCATOR scalings.

A schematic drawing of the DWT mode transport coefficients is given in Fig. 1.

3.2. Empirical, anomalous transport models

In helical systems the transport process is anomalous, as in tokamaks, and the empirical scaling of the global confinement time $\tau_{E,emp}$(s) for helical systems (so-called LHD scaling [5]) is given by

$$\tau_{E,emp} = 0.17 f_{enh} P_{MW}^{-0.58} n_{20}^{0.69} B_T^{0.84} R_m^{0.75} a_m^2 \quad (31)$$

where P_{MW} is the total absorbed heating power (MW), n_{20} is the average plasma density (10^{20} m^{-3}), B_T is the magnetic field strength (T), R_m is the major plasma radius (m) and a_m is the minor plasma radius (m). We take into account the confinement improvement by an enhancement factor f_{enh}. For the local transport coefficient $\chi(\rho)$ (m^2/s) as a function of the flux averaged radial variable ρ, the Heliotron-E scaling [9] near the position of $r/a_p = 2/3$ (a_p: plasma radius) was deduced as

$$\chi_{H\text{-}E}(\rho) = 30.6 B_T^{-2.0} T_{keV}(\rho)^{1.52} \quad (32)$$

On the other hand, the WVII-AS semi-local χ scaling [10] was derived by using the total absorbed heating power P:

$$\chi_{W7\text{-}AS}(\rho) = 0.64 P_{MW}^{0.76} B_T^{-0.60} n_{20}(\rho)^{-0.95} \iota^{-0.49} \quad (33)$$

The former $\chi(\rho)$ scaling is only valid in the half-radius region, and both scalings do not include the major radius dependence which is important for estimating the performance of future machines.

By using the relation $\chi(\rho) \sim \rho^2/4\tau_E(\rho)$, we define a new scaling for semi-local thermal diffusivity as a combination of the $n(\rho)$&$T(\rho)$ dependent diffusivity $\chi_1(\rho)$ and the $n(\rho)$ dependent diffusivity $\chi_2(\rho)$ with the P dependent coefficient:

$$\chi_{emp}(\rho) = \chi_1^s \chi_2^{(1-s)} \quad (34)$$

$$\chi_1(\rho) = 15.8 f_{enh}^{-2.38} B_T^{-2.0} R_m^{-0.40} T(\rho)_{keV}^{1.38} n_{20}(\rho)^{-0.26} \quad (35)$$

$$\chi_2(\rho) = 1.47 f_{enh}^{-1} P_{MW}^{0.58} B_T^{-0.84} R_m^{-0.75} n_{20}(\rho)^{-0.69} \quad (36)$$

where s is an adjusting parameter to fit the experimental data. The radial profile of $\chi_1(\rho)$ decreases outwards owing to the temperature dependence and does not reproduce the experimental profile data. On the other hand, the coefficient $\chi_2(\rho)$ depends only on the density

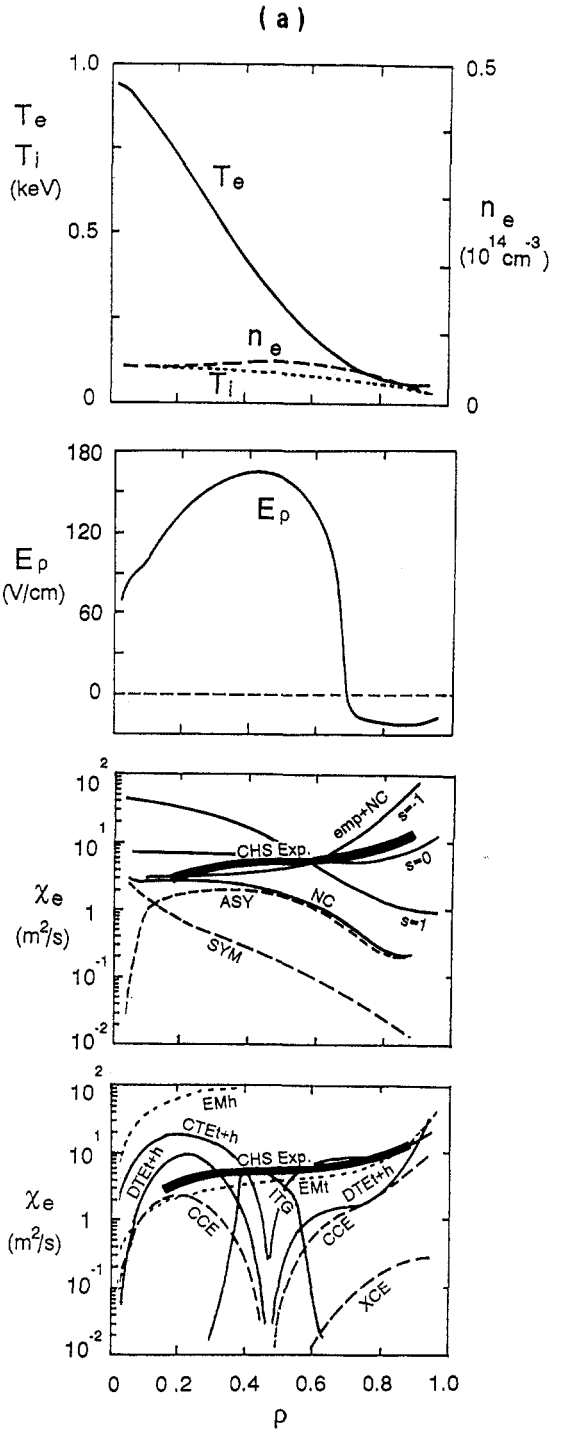

FIG. 2. Comparison of modelled thermal conductivities with experimental data from the CHS [8]. The density and temperature profiles are obtained from experimental data, and the radial electric field profiles are calculated using the ripple transport model. The experimental diffusivity (CHS Exp.) is compared with the semi-empirical model combined with neoclassical transport (emp + NC) with several s values. The drift wave models are also compared.
(a) Low density ECH.

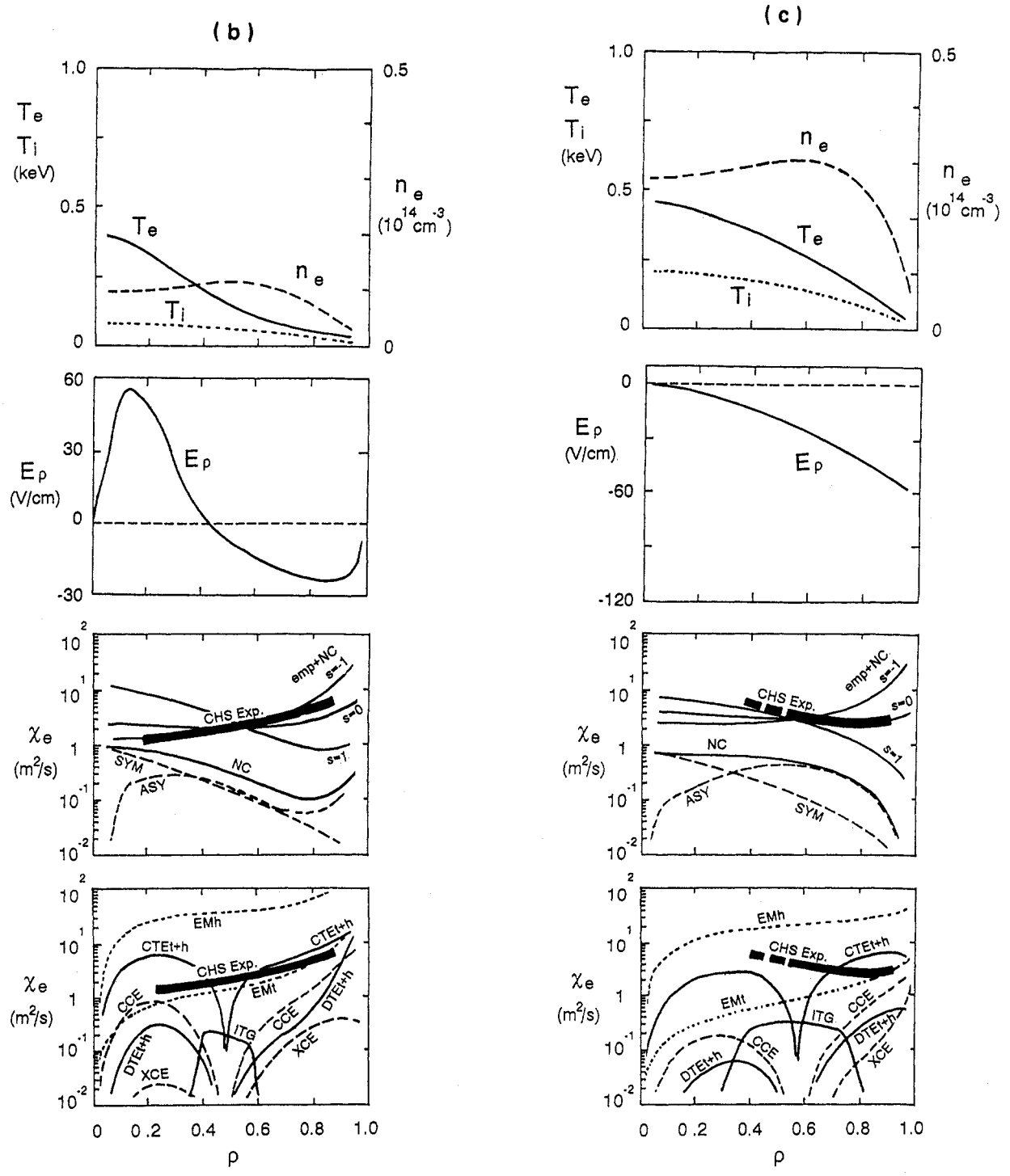

FIG. 2. Comparison of modelled thermal conductivities with experimental data from the CHS [8]. The density and temperature profiles are obtained from experimental data, and the radial electric field profiles are calculated using the ripple transport model. The experimental diffusivity (CHS Exp.) is compared with the semi-empirical model combined with neoclassical transport (emp + NC) with several s values. The drift wave models are also compared. (b) Medium density ECH and (c) NBI heating.

profile and increases outwards, but it still disagrees with the experimental data. The proper s value is $0 \lesssim s \lesssim 0.5$, as shown in Section 4. The ECH plasma with the neoclassical transport in the centre and anomalous transport in the outer region corresponds to $s \sim 0.3$–0.5. The anomalous transport in the whole region of NBI plasmas is described by $s \sim 0$–0.2. The semi-local coefficient can reproduce the experimental profiles.

In another model, the spatial factor $g(\rho)$ is added to the averaged transport coefficient $\langle\chi_1(\rho)\rangle$:

$$\chi_{emp}(\rho) = \langle\chi_1(\rho)\rangle\, g(\rho) \tag{37}$$

$$g(\rho) = \frac{\nu + 1}{\mu + \nu + 1}(1 + \mu\rho^{2\nu})$$

The coefficients can be chosen to fit the experimental data. Typically, $\mu = 10$ and $\nu = 4$ are used in this paper.

4. COMPARISON WITH EXPERIMENTAL DATA FROM CHS

The transport coefficients described in the previous section are compared with typical experimental data of two ECH plasma discharges and one NBI heated discharge [8] in the Compact Helical System (CHS, helical period M = 8, major radius R = 1.0 m, magnetic field B = 1.5 T). The experimentally obtained density and temperature profiles of low density and medium density ECH discharges are approximated by the following forms:

(a) Low n_e ECH case (0.9 T magnetic field, 180 kW absorbed heating power):

$$n_e[10^{12}\ cm^{-3}] = (4.0 - 0.5)(1 - \rho^2)^{1.5}(1 + 3.5\rho^2) + 0.5$$

$$T_e[eV] = (900\text{-}100)(1 - \rho^{1.5})^3 + 100$$

$$T_i[eV] = (100\text{-}20)(1 - \rho^2) + 20$$

(b) Medium n_e ECH case (0.95 T magnetic field, 63 kW absorbed heating power):

$$n_e[10^{12}\ cm^{-3}] = (8.0\text{-}1.0)(1 - \rho^2)^{1.5}(1 + 3.5\rho^2) + 1.0$$

$$T_e[eV] = (400\text{-}50)(1 - \rho^{1.5})^3 + 50$$

$$T_i[eV] = (80\text{-}10)(1 - \rho^2) + 10$$

(c) NBI case (1.5 T, 1.1 MW, NBI): The profile of an NBI heated discharge is given by

$$n_e[10^{13}\ cm^{-3}] = (2.5\text{-}0.5)(1 - \rho^4)(1 + \rho^2) + 0.5$$

$$T_e[eV] = (450\text{-}20)(1 - \rho^{1.5}) + 20$$

$$T_i[eV] = (200\text{-}20)(1 - \rho^2) + 20$$

All these density profiles are hollow. The calculated transport coefficients are shown in Fig. 2 and compared with experimental data. The neoclassical values of the symmetric (SYM) and asymmetric (ASY) transport parts are also shown. The radial electric field E_ρ plotted in this figure is obtained from Eq. (8). These calculated radial electric fields agree with experimental values in the plasma core except near the plasma surface [24]. The helical ripple asymmetric transport near the edge may be smaller than in Fig. 2 because the electric field may be higher than expected. The ripple transport estimated here includes multiple helicity of the magnetic field components and therefore it is larger than the estimated transport from single helicity given in Ref. [8]. The radial electric field for low density ECH plasmas is positive, and the 'electron root' solution is obtained. On the other hand, for NBI heated higher density plasmas, the electric field becomes negative and the 'ion root' solution is obtained. From Fig. 2 it is apparent that the experimental electron thermal conductivity near the plasma centre is neoclassical for ECH plasmas, while for NBI plasmas the transport is anomalous in the whole plasma region. For the anomalous empirical transport model combined with the neoclassical model, the best fitting s value for low density ECH plasma (Fig. 2(a)) is -0.4 and the obtained diffusivity is

$$\chi_{emp}(\rho) = 0.57 f_{enh}^{-0.45} P_{MW}^{0.81} B_T^{-0.38} R_m^{-0.89} T_{keV}(\rho)^{-0.55} n_{20}(\rho)^{-0.86} \tag{38}$$

The optimal s value for NBI heated plasmas (Fig. 2(c)) is 0 and the resultant diffusivity is

$$\chi_{emp}(\rho) = 1.47 f_{enh}^{-1} P_{MW}^{0.58} B_T^{-0.84} R_m^{-0.75} n_{20}(\rho)^{-0.69} \tag{39}$$

For the DWT models, the diffusivity of the collisionless trapped electron mode due to toroidicity (CTEt) is almost the same as that due to helicity (CTEh), and the total CTE mode combined with the ITG mode agrees roughly with the experimental data. However, with the present CHS parameters, the CTE modes are stabilized and dissipative (DTE) modes are dominant since $\nu_{efft} > \omega_{*e}$. The electrostatic dissipative DWT transport combined with ITG modes does not explain the experimental data, in contrast to ATF results [6].

The electromagnetic mode related with toroidicity (EMt) is close to the experimental transport coefficient for ECH plasmas. The mode for helical ripple (EMh) adopted here is too large and is unrealistic. For NBI heated plasmas, even the EM mode does not fit the experiments near the centre.

5. TRANSPORT SIMULATIONS FOR THE LHD

5.1. Simulation model

For the analysis of the LHD transport, a 2-D equilibrium transport code has been developed in which the 3-D equilibrium code VMEC [25] and the 1-D transport code HTRANS are used. The NBI deposition is calculated by the HFREYA code, which is a helical modification of FREYA [26], and the slowing down calculation is done with the Fokker–Planck code FIFPC [27]. The neoclassical and anomalous transports described in Sections 2 and 3 are used. The schematic flow chart of this simulation code is shown in Fig. 3.

5.1.1. Equilibrium analysis

The initial vacuum magnetic surface is calculated by the magnetic tracing code HSD [28] with carefully arranged multi-filament currents. In the paper, the fixed boundary version of VMEC is used. The FCT and bootstrap currents are not included; these currents are estimated to be not large enough to affect the present transport analysis. A full transport simulation which employs the free boundary VMEC code and includes the current equation is in progress. The 3-D magnetic field obtained by the finite beta equilibrium of VMEC is used to evaluate the NBI heat deposition and the multi-helicity neoclassical coefficients.

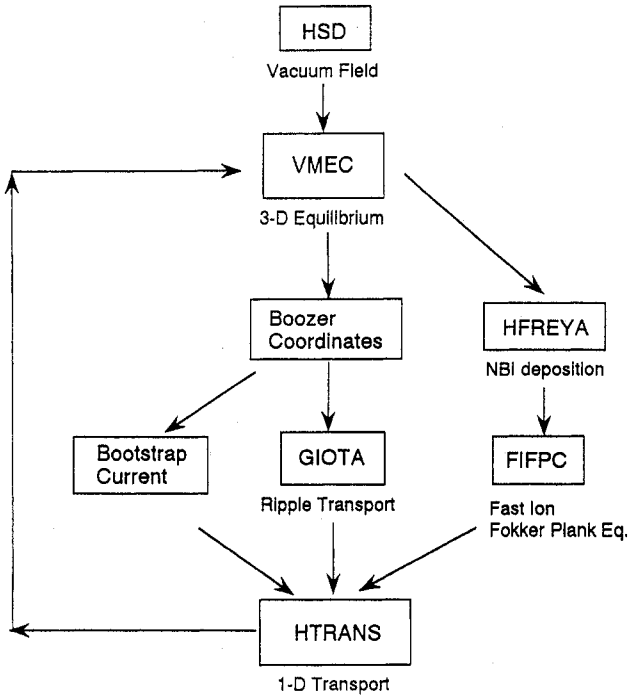

FIG. 3. Flow chart of the equilibrium transport simulation analysis. The 3-D equilibrium VMEC code is coupled in the FCT manner to the 1-D transport code HTRANS including the neoclassical ripple transport code GIOTA and various NBI heating codes.

5.1.2. Transport equations

The 1-D particle and energy fluid transport equations have the general forms:

$$\frac{\partial n_e}{\partial t} = -\frac{1}{V'(\rho)}\frac{\partial}{\partial \rho}\left[V'(\rho)\Gamma_e\right] + S_e - \Gamma_{\|e}/L_\| \quad (40)$$

$$\frac{\partial}{\partial t}\left(\tfrac{3}{2} n_e T_e\right) = -\frac{1}{V'(\rho)}\frac{\partial}{\partial \rho}\left[V'(\rho)\left(Q_e + \tfrac{5}{2} T_e \Gamma_e\right)\right] - \Gamma_e E_\rho - P_{ei} + P_{He} - P_{rad} - Q_{\|e}/L_\| \quad (41)$$

$$\frac{\partial}{\partial t}\left(\tfrac{3}{2} n_i T_i\right) = -\frac{1}{V'(\rho)}\frac{\partial}{\partial \rho}\left[V'(\rho)\left(Q_i + \tfrac{5}{2} T_i \Gamma_i\right)\right] + \Gamma_i E_\rho + P_{ei} + P_{Hi} - P_{cx} - Q_{\|i}/L_\| \quad (42)$$

where S_e denotes the particle source due to neutral beam fuelling and feedback controlled gas puffing as calculated by the Monte Carlo code AURORA [29]. The variables P_{He} and P_{Hi} are the input heating power to electrons and ions from the neutral beam calculated by the Fokker–Planck code [27] and/or the radio-frequency heating. P_{ei}, P_{rad} and P_{cx} are the electron–ion power exchange, the radiation power loss and the charge exchange power loss, respectively. The particle flux Γ and the heat flux Q are defined by using the diffusion coefficient D and the thermal diffusivity χ:

$$\Gamma_e = \Gamma_{ASYe} - (D_{SYMe} + D_{ANe})\langle|\nabla\rho|^2\rangle\frac{\partial n_e}{\partial \rho} \quad (43)$$

$$Q_e = Q_{ASYe} - (\chi_{SYMe} + \chi_{ANe}) n_e \langle|\nabla\rho|^2\rangle\frac{\partial T_e}{\partial \rho} \quad (44)$$

$$Q_i = Q_{ASYi} - (\chi_{SYMi} + \chi_{ANi}) n_i \langle|\nabla\rho|^2\rangle\frac{\partial T_i}{\partial \rho} \quad (45)$$

The particle and heat flux to the limiter or divertor is related to the sound velocity C_s multiplied by the coefficients α (0.2–1.0) and γ ($\sim$2.9):

$$\Gamma_\| = n_e \alpha C_s \quad (46)$$

$$Q_{\|e} = 2\gamma n_e T_e \alpha C_s \quad (47)$$

$$Q_{\|i} = 2 n_i T_i \alpha C_s \quad (48)$$

which determine the plasma edge temperature, with an assumed wall temperature (typically $\sim$10 eV).

5.2. Simulation for LHD plasmas

The LHD magnetic configuration [3, 4] is characterized by the $\ell = 2$ heliotron/torsatron with a continuous helical coil system. The major radius is 4 m (finally determined to be 3.9 m) and the magnetic field strength is 4 T. The winding law of the helical coil with the major radius R_c and the minor radius a_c is

$$\theta = \frac{m}{\ell}\phi + \alpha_c \sin\left(\frac{m}{\ell}\phi\right)$$

$$\gamma_c = \frac{m a_c}{\ell R_c}$$

where γ_c is the coil pitch parameter, α_c is the pitch modulation parameter, and θ and ϕ are the poloidal and toroidal co-ordinates, respectively. Three sets of poloidal coils are used to produce various shapings of the plasma cross-section, and three block layers of helical coils are energized to change the γ value for the control of the plasma size and the divertor layer. A schematic cross-section of the LHD machine is shown in Fig. 4. Typical simulation results of 20 MW NBI heated LHD plasmas using the electron anomalous transport model of Eq. (37) are shown in Fig. 5 for low density and high density discharges. Anomalous inward flows of particles are not included in the simulations. The density profiles obtained are flat or hollow. Such hollow density profiles are seen in many of the existing experiments. For electron thermal transport the empirical thermal conductivity exceeds the neoclassical value; on the other hand, for ion energy transport the neoclassical helical ripple contribution cannot be neglected. Typical predictions from the DWT model with neoclassical transport are presented in Ref. [3].

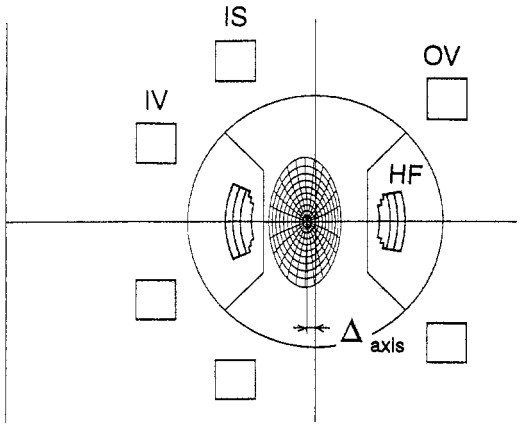

FIG. 4. LHD machine configuration and plasma equilibrium. Helical pitch M = 10, major radius R = 4.0 m, toroidal field B = 4.0 T.

Because of the flat density profile, the ITG mode is dominant in the ion transport process of the plasma core, instead of the CTE, DTE, CCE and XCE modes.

To assess the ripple transport effects, the simulation results without and with ripple transport are compared in Fig. 6(a) and (b). The confinement time derived from the simulation, τ_E, and the corresponding simple estimation from Eq. (32), $\tau_{E,emp}$, are compared. Inclusion of the ripple transport loss leads to a 20% reduction in the global confinement time. The average temperature is not different in the two cases, but the central ion temperature is decreased by 20%. The central density is decreased owing to the ripple diffusion process. By changing the magnetic configuration from (b) $\alpha_c = 0$ to (c) $\alpha_c = 0.1$, the plasma radius defined by the last closed flux surface is increased from 0.50 cm to 0.55 cm for the case of the inward axis shift $\Delta_{axis} = -0.1$ m. This moderate positive pitch modulation of the helical coil reduces the central temperature by 20% because of high ripple ion loss, but it leads to a slight increase in the plasma radius and, hence, an increase in the global confinement. Moreover, the positive α_c configuration with a higher effective helical ripple provides easier access to the hot ion regime with a positive electric field at low density operation, as shown in Fig. 5(a). The final magnetic configuration for the LHD with moderate positive α_c was determined by physics criteria [3] for beta, high energy particle orbit confinement, divertor configuration and plasma transport, and also by criteria for engineering constraints [28].

The inward shift of the plasma column is effective in reducing the ripple transport and improving the plasma confinement in the LHD; this has been demonstrated in several recent helical device experiments. In our simulation, the reduction of the ripple loss is included (see Section 2). The achievable fusion product $nT\tau_E$ is plotted as a function of the magnetic axis shift Δ_{axis} for several enhancement factors f_{enh} in Fig. 7, where the anomalous model of Eq. (39) for electrons and ions is adopted. The plasma dominated by neoclassical loss with $f_{enh} = 10$ is obviously improved by the inward shift ($nT\tau_E$ is almost twice as much). For $f_{enh} = 1$ the fusion product $nT\tau_E$ increases by 50% with an inward axis shift of 0.2 m.

6. SUMMARY

We have developed a new 3-D equilibrium/1-D transport simulation model for helical confinement systems in order to predict the behaviour of LHD plasmas. For the transport processes, we have considered the neoclassical transport theory, including the effects of the radial electric field and the multi-helicity magnetic components,

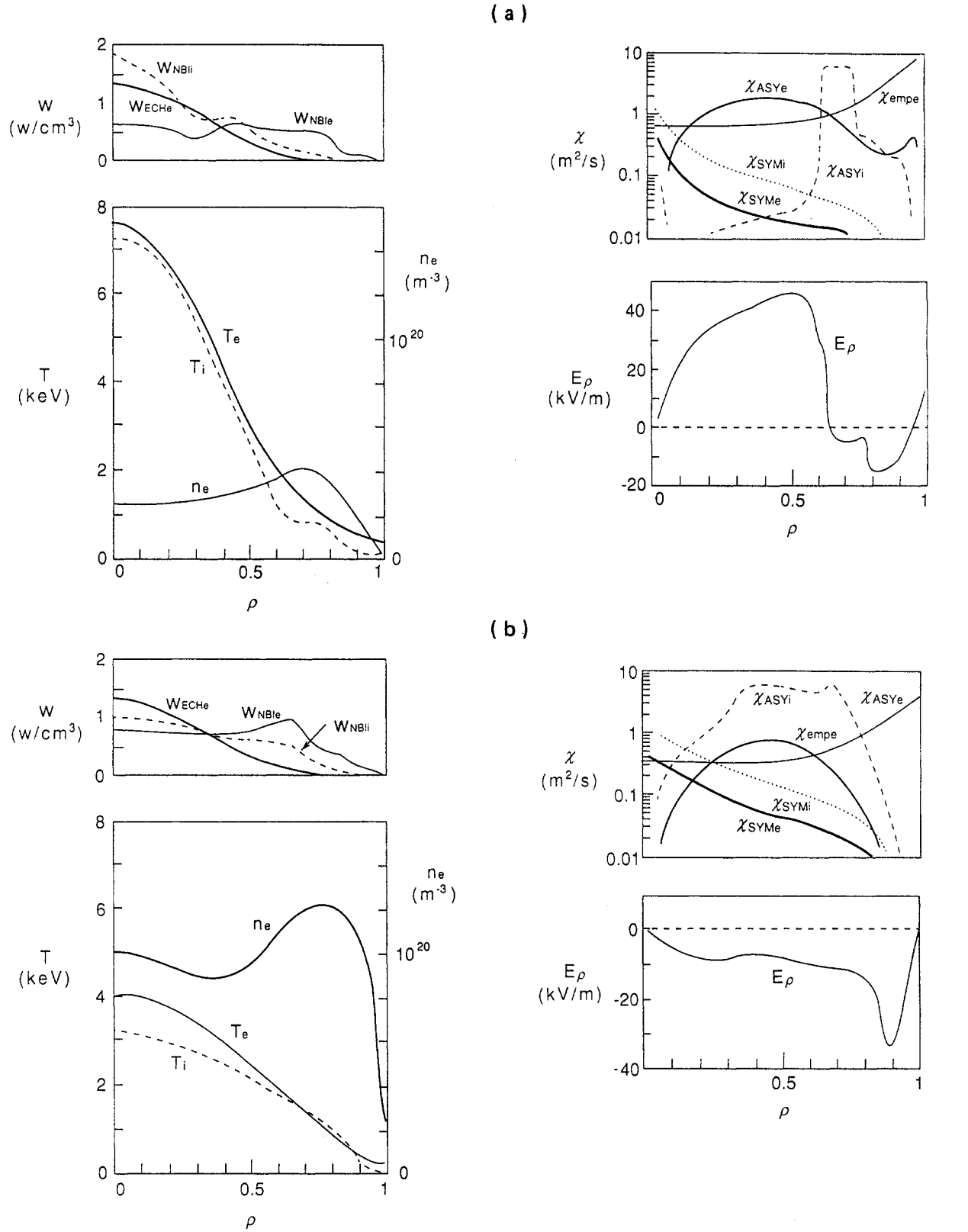

FIG. 5. Transport simulations of LHD plasmas with 20 MW NBI heating using the anomalous loss model of Eq. (37) for electrons. In addition to the simulation results, the corresponding empirical global confinement times $\tau_{E,emp}$ estimated from Eq. (32) are plotted. (a) Low density case with a positive electric field (electron root), average electron density 3.0 × 10^{19} m^{-3}. (b) High density case with a negative electric field (ion root), average electron density 1.0 × 10^{20} m^{-3}.

(a)

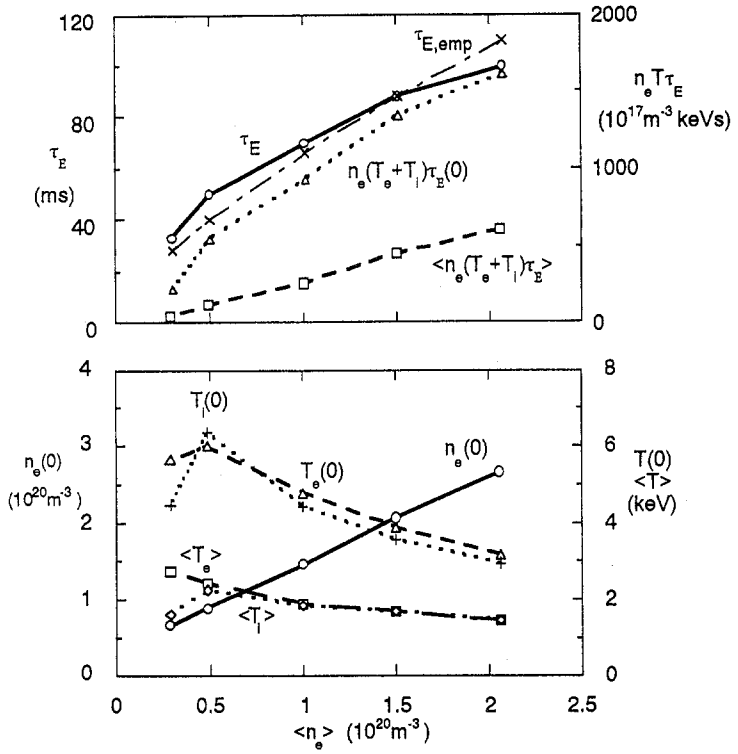
120
80
40
0
τ_E (ms)
2000
1000
0
$n_e T\tau_E$ (10^{17}m^{-3} keVs)
$\tau_{E,emp}$
τ_E
$n_e(T_e+T_i)\tau_E(0)$
$\langle n_e(T_e+T_i)\tau_E\rangle$
4
3
2
1
0
$n_e(0)$ (10^{20}m^{-3})
8
6
4
2
0
T(0) <T> (keV)
$T_i(0)$
$T_e(0)$
$n_e(0)$
$\langle T_e\rangle$
$\langle T_i\rangle$
0
0.5
1
1.5
2
2.5
$\langle n_e\rangle$ (10^{20}m^{-3})

(b)

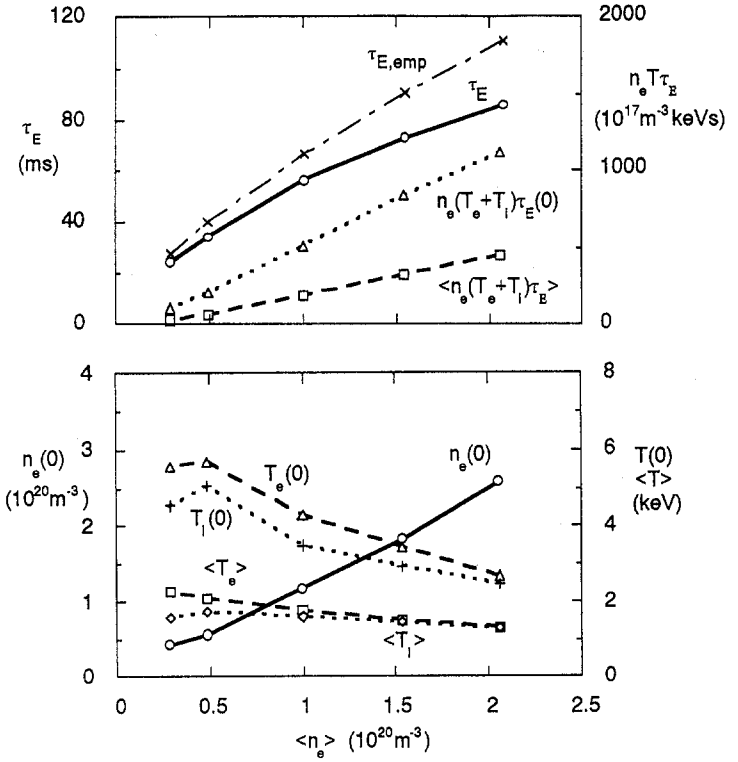
120
80
40
0
τ_E (ms)
2000
1000
0
$n_e T\tau_E$ (10^{17}m^{-3} keVs)
$\tau_{E,emp}$
τ_E
$n_e(T_e+T_i)\tau_E(0)$
$\langle n_e(T_e+T_i)\tau_E\rangle$
4
3
2
1
0
$n_e(0)$ (10^{20}m^{-3})
8
6
4
2
0
T(0) <T> (keV)
$T_e(0)$
$T_i(0)$
$n_e(0)$
$\langle T_e\rangle$
$\langle T_i\rangle$
0
0.5
1
1.5
2
2.5
$\langle n_e\rangle$ (10^{20}m^{-3})

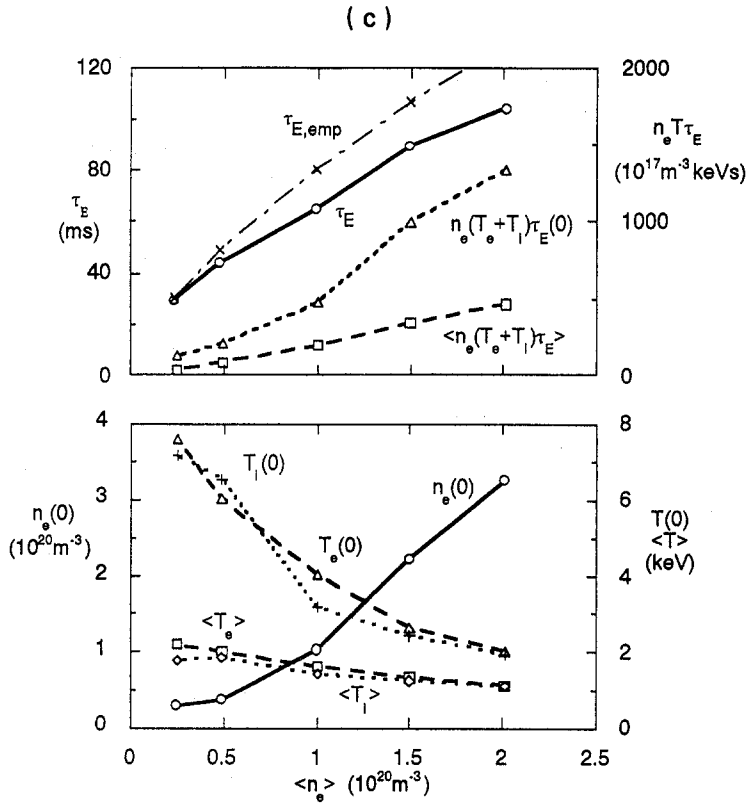

FIG. 6. Effects of the helical ripple transport and the magnetic configuration for the electron anomalous loss model of Eq. (37).
(a) Without helical ripple diffusion; the empirical anomalous model with symmetric neoclassical transport is taken into account.
(b) Standard configuration (α_c = 0.0) with empirical anomalous loss and neoclassical total loss.
(c) Positive helical pitch modulation (α_c = 0.1) with empirical anomalous loss and neoclassical total loss.

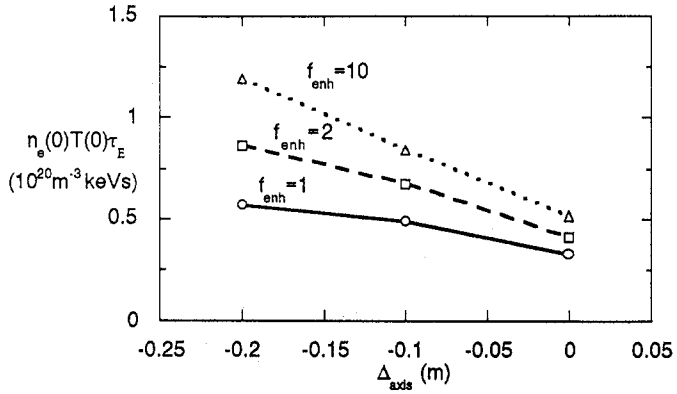

FIG. 7. Effects of the radial inward shift Δ_{axis} and the confinement enhancement factor f_{enh} on the central value of the fusion product $n(0)\,T(0)\,\tau_E$. The anomalous transport model of Eq. (39) is used for both electrons and ions.

and the drift wave turbulence transport for electrostatic and electromagnetic modes, or the anomalous semi-empirical transport. These electron thermal diffusivities have been compared with experimental data from the CHS. Our conclusions are summarized as follows:

(1) From the comparison between the CHS experiment and the present model, we have found that the central transport coefficient of the ECH plasma agrees with the neoclassical axisymmetric value, and the transport outside the half-radius is anomalous. On the other hand, the transport of NBI heated plasmas is anomalous in the whole plasma region. It is impossible to completely explain this anomaly by electrostatic DWT models such as dissipative trapped electron modes for CHS flat density profile discharges.

(2) In the LHD simulation it has been clarified that the global confinement time is sensitive to the electron anomalous transport. The effect of the neoclassical transport on the global confinement time is about 10%; however, the central ion temperature can be raised by 20% by reducing the ripple transport. If the anomalous loss can be reduced to half of the value used in the present scaling, as is the case in the H-mode of tokamak discharges, the neoclassical ripple loss through the ion channel becomes important even in the plasma core.

(3) The reduction of anomalous loss is important in the LHD. The moderate positive pitch modulation required to increase the plasma radius is more effective in improving the global confinement than well arranged and optimized configurations of the neoclassical transport.

(4) The radial inward shift of the plasma column improves the ion confinement and raises the central ion temperature by reducing the neoclassical asymmetric ion transport loss and increasing the plasma radius. This transport reduction is due to the modification of the satellite magnetic structure by the radial shift of the plasma. Such a reduction can also be achieved by other means, for example by varying the winding law of helical coils [30–32].

ACKNOWLEDGEMENTS

The authors would like to thank Dr. S.P. Hirshman for providing the VMEC code and Dr. C.L. Hedric for the GIOTA code. They also wish to thank Dr. Y. Ogawa for discussing DKES code results, and Drs. H. Yamada, H. Iguchi, K. Ida and K. Matsuoka for discussing CHS experimental data. They are grateful to Drs. O. Motojima, M. Fujiwara and A. Iiyoshi for continuous encouragement.

REFERENCES

[1] LYON, A., Fusion Technol. **17** (1990) 17.
[2] IIYOSHI, A., FUJIWARA, M., MOTOJIMA, O., OHYABU, N., YAMAZAKI, K., Fusion Technol. **17** (1990) 169.
[3] YAMAZAKI, K., OHYABU, N., OKAMOTO, M., et al., in Plasma Physics and Controlled Nuclear Fusion Research 1990 (Proc. 13th Int. Conf. Washington, DC, 1990), Vol. 2, IAEA, Vienna (1991) 709.
[4] MOTOJIMA, O., AKAISHI, K., ASAO, M., et al., ibid., Vol. 3, p. 513.
[5] SUDO, S., TAKEIRI, Y., ZUSHI, H., et al., Nucl. Fusion **30** (1990) 11.
[6] MURAKAMI, M., ACETO, S.C., ANABITARTE, E., et al., in Plasma Physics and Controlled Nuclear Fusion Research 1990 (Proc. 13th Int. Conf. Washington, DC, 1990), Vol. 2, IAEA, Vienna (1991) 455.
[7] ZUSHI, H., WAKATANI, M., TAKEUCHI, K., et al., Nucl. Fusion **24** (1984) 305.
[8] IGUCHI, H., HOSOKAWA, M., HOWE, H.C., et al., in Controlled Fusion and Plasma Heating (Proc. 16th Eur. Conf. Amsterdam, 1990), Vol. 14B, Part II, European Physical Society (1990) 451.
[9] SANO, F., TAKEIRI, Y., HANATANI, K., et al., Nucl. Fusion **30** (1990) 81.
[10] RINGLER, H., GASPARINO, U., KUHER, G., et al., Plasma Phys. Control. Fusion **32** (1990) 933.
[11] HINTON, F.L., HAZELTINE, R.D., Rev. Mod. Phys. **48** (1976) 239.
[12] SHAING, K.C., CALLEN, J.D., Phys. Fluids **26** (1983) 3315.
[13] CHANG, C.S., HINTON, F.L., Phys. Fluids **25** (1982) 1493.
[14] CRUME, E.C., SHAING, K.C., HIRSHMAN, S.P., Van RIJ, W.I., Phys. Fluids **31** (1988) 11.
[15] HASTINGS, D.E., HOULBERG, W.A., SHAING, K.C., Nucl. Fusion **25** (1985) 445.
[16] SHAING, K.C., HORKIN, S.A., Phys. Fluids **26** (1983) 2136.
[17] HEDRIC, C.L. (ORNL), personal communication on the GIOTA code, 1988.
[18] HIRSHMAN, S.P., SHAING, K.C., Van RIJ, W.I., BEASLEY, C.O., CRUME, E.C., Phys. Fluids **29** (1986) 2951.
[19] PERKINS, F.W., in Heating in Toroidal Plasmas (Proc. 4th Int. Symp. Rome, 1984), Vol. 2, Monotypia Franchi, Perugia (1984) 977.
[20] DOMINGUEZ, R.R., WALTZ, R.E., Nucl. Fusion **27** (1987) 65.
[21] GOLDSTON, R., Bull. Am. Phys. Soc. **34** (1989) 1964.
[22] HORTON, W., BEKKI, N., BERK, L.H., et al., in Plasma Physics and Controlled Nuclear Fusion Research 1988 (Proc. 12th Int. Conf. Nice, 1988), Vol. 2, IAEA, Vienna (1989) 211.
[23] OHKAWA, T., Phys. Lett., A **67** (1978) 35.
[24] IDA, K., YAMADA, H., IGUCHI, H., HIDEKUMA, S., SANUKI, H., YAMAZAKI, K., CHS Group, Phys. Fluids B **3** (1991) 515.
[25] HIRSHMAN, S.P., Van RIJ, W.I., MERKEL, P., Comput. Phys. Commun. **43** (1986) 143.
[26] LISTER, G.G., POST, D.E., GOLDSTON, R., in Plasma Heating in Toroidal Devices (Proc. 3rd Symp. Varenna, 1976), Editrice Compositori, Bologna (1976) 303.
[27] FOWLER, R.H., SMITH, J., ROME, J.A., Comput. Phys. Commun. **13** (1978) 323.
[28] YAMAZAKI, K., MOTOJIMA, O., ASAO, M., Fusion Technol. **21** (1992) 147.
[29] HUGES, M.H., POST, D.E., J. Comput. Phys. **28** (1978) 43.
[30] BYKOV, V.E., GEORGIEVSKIJ, A.V., PELETMINSKAYA, V.G., KHODYACHIKH, A.V., SHISHKIN, A.A., Nucl. Fusion **24** (1984) 1195.
[31] BEIDLER, C.D., HITCHON, W.N.G., GREKOV, D.L., SHISHKIN, A.A., Nucl. Fusion **30** (1990) 405.
[32] TODOROKI, J., Phys. Soc. Jpn. **59** (1990) 2758.

(Manuscript received 24 July 1991
Final manuscript received 2 December 1991)